

Revised Proposal

Direct measurements of ω mass modification in $A(\pi^-, n)\omega X$ reaction and $\omega \rightarrow \pi^0\gamma$ decays

January 7, 2010

K. Ozawa¹, K. Utsunomiya, Y. Watanabe, Y. Komatsu,
S. Masumoto, and R.S. Hayano

Physics department, Graduate School of Science, University of Tokyo

S. Yokkaich, K. Aoki

RIKEN

Y. Morino

RCNP, Osaka University

¹Contact person, e-mail:ozawa@phys.s.u-tokyo.ac.jp

Contents

1	Summary of the existing proposal	3
1.1	Physics Goal	3
1.2	Experimental Apparatus	5
2	Existing experimental results	6
3	Neutron counter	9
3.1	Beam test for large scintillator	9
3.2	Neutron detection efficiency	11
4	Gamma-ray detector and simulation study	13
4.1	Existing data	13
4.2	Simulation tuning	14
4.3	Fiducial cut	19
4.4	Invariant mass evaluation	19
4.5	Detector acceptance	20
5	Yield and mass spectrum	22
5.1	Theoretical cross section calculation	22
5.2	Yield calculation	23
5.3	Expected missing mass spectrum	25
5.4	Expected invariant mass spectrum	27
5.5	Final yield for physics	28
6	Background estimation	29
7	Final state interaction	31
8	Trigger	32
9	Additional Target	33
10	Cost estimation	34
11	Summary	35
	References	36

1 Summary of the existing proposal

1.1 Physics Goal

The origin of the hadron mass has been drawing strong interests in nuclear and particle physics. Especially in QCD, mass of hadrons is composed of a sum of the effective mass of valence quarks, known as constituent quark mass, and their interaction term. According to theoretical models, the effective mass of valence quarks is determined by chiral property of QCD vacuum. This mechanism is understood as a consequence of the dynamical breaking of chiral symmetry. In hot and/or dense matter, this broken symmetry will be restored either partially or completely and, hence, properties of hadrons, such as mass, decay modes and life time, can be modified. Therefore, we can study the origin of hadron mass and chiral properties of QCD medium by measuring in-medium properties of mesons. Especially, mass spectra of vector mesons is directly connected to anti-quark quark condensates [1], which is an order parameter of chiral symmetry. Relatively large mass modification is theoretically expected even at nuclear density [2]. Thus, we focus on ω meson mass in nucleus in this propose experiment.

Mass of ω meson at finite density, such as nucleus, has been studied in many theoretical methods. Hatsuda and Lee studied using a QCD sum rule and partial chiral symmetry restoration. They predicted 10~20% decreasing for ρ/ω mass at normal nuclear density [1]. Klingl *et al.* calculated the downward mass-shift and even mass broadening of $\rho/\omega/\phi$ in dense matter [3]. Some models considered couplings to baryon resonances and predicted broadening and slight increasing of ω mass [4, 5].

There are several theoretical activities, however, there is no conclusive result experimentally. The main purpose of the proposed experiment is measurements of direct ω mass modification under a clear condition. Decays of ω meson in nucleus are measured with $\omega \rightarrow \pi^0\gamma$ mode and initial conditions of produced ω meson are also measured in $A(\pi^-, n)\omega$ reaction. Fig.1 shows a schematic view of combined measurements. Using missing mass information in forward neutron measurements, the generation process of ω meson can be identified. In addition, ω meson is generated in recoil less kinematics and the momentum of generated ω meson is very limited within the Fermi motion. Also, if ω meson is bounded in nucleus, which can be observed using the forward neutron measurement, the kinematical condition of ω meson in nucleus is established very clearly.

Besides such physics advantages, there is an experimental advantage. Simultaneous measurements can reduce a combinatorial background strongly. Evaluation of combinatorial background is a major issue in the direct mass

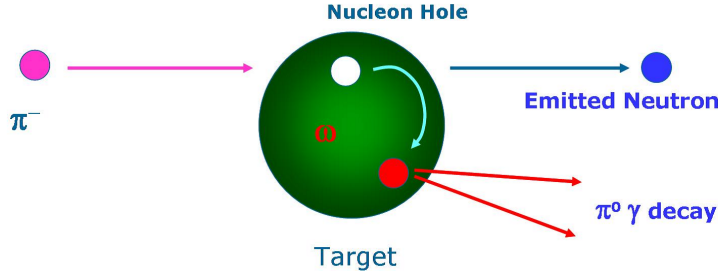


Figure 1: Schematic view of combined measurements

measurements via decays. M. Kaskulov *et al.* claims that TPAS results [6] are not robust under shape difference of combinatorial background [7]. In the proposed experiment, combined measurements can achieve small background measurements.

In addition, nuclear ω bound states can be measured in $A(\pi^-, n)\omega$ reaction, if the bound state exists. This is the first measurement to see ω bound state in nucleus. Calculations about possible ω bound states have been developed by several groups. W. Weise and his group predict 30 MeV binding energy [8]. H. Nagahiro *et al.* predict 50 MeV binding energy using an optical potential method [7, 9]. Fig.2 shows a prediction of ω bound state from [9].

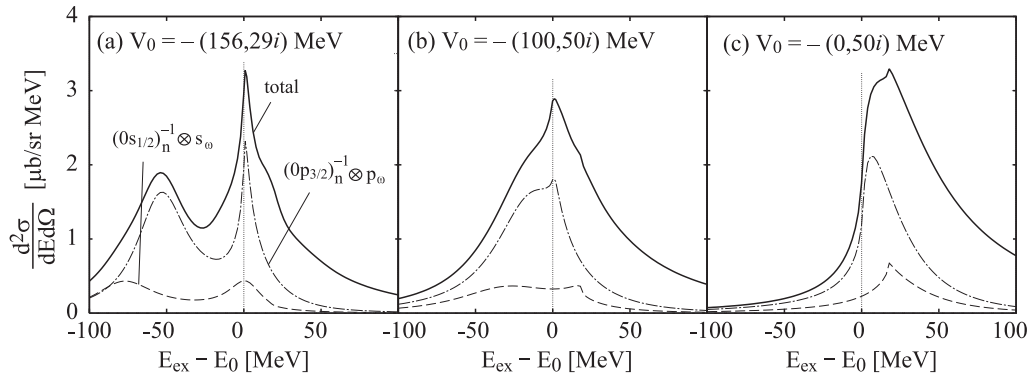


Figure 2: Calculated spectra of $^{12}\text{C}(\pi^+, p)^{11}\text{C} \otimes \omega$ reaction as functions of the excited energy E_{ex} . E_0 is the ω production threshold. The neutron-hole states are indicated as $(nl_j)_n^{-1}$ and the ω states as l_ω [9].

When a binding energy of a ω bound state in nucleus is measured, it can be interpreted to optical potential and gives a phenomenological information about interactions between ω meson and nuclei. If mass distribution of bounded ω meson is measured directly via decays, the relation between

mass distribution and nuclear-meson interaction is established experimentally. Then, the amount of ω mass shift in direct mass spectrum and ω binding energy can be compared. Such comparison gives information about effects beyond the meson nuclei interaction, such as chiral symmetry restoration.

1.2 Experimental Apparatus

We measured $A(\pi^-, n)\omega$ reaction with forward neutron measurements and decays of generated ω meson with $\omega \rightarrow \pi^0\gamma$ mode and π^0 meson is detected with 2 γ decays. In the measurements, two detectors are needed. One is neutron counter at the forward region and another is gamma-ray detector for detecting 3 γ 's at target region. Thickness of 6 cm of Carbon-12 is chosen as a target to maximize ω yield. The beam momentum of 1.8 GeV is chosen to have recoil less production of ω meson and obtain clear bound state in nucleus. To achieve the required beam momentum, K1.8 beam line needs to be used. The beam intensity of 10^7 per spill is also required to collect reasonable amount of yield, as described later. Momentum of incident π^- beam is measured by tracking devices at the beam line. The resolution of missing mass measurements is mainly determined by the resolution of forward neutron momentum measurements and the required resolution for π^- momentum is about 1%.

We measure incident π^- meson and forward neutron in $A(\pi^-, n)X$ reaction and calculate missing mass to identify ω meson production. The forward neutron momentum is measured using newly constructed neutron counter and time of flight method. Emitted neutron should be detected at 0 degree to minimize momentum transfer to ω meson. Produced charged particles as a background and π^- beam are swept by a magnet. The SKS magnet can be used for such sweeping. Details of updated neutron detector are described later.

Decays of ω meson are measured using $\omega \rightarrow \pi^0\gamma$ mode and π^0 meson is detected with 2 γ decays. Thus, total 3 γ 's need to be detected. The ω meson is generated almost at rest and decayed γ and π^0 goes to back to back. Thus, large acceptance is needed to the γ detection. We are planning to use existing gamma-ray detector, which has 75% acceptance and consists of CsI crystals. The gamma-ray detector is used at KEK E246 experiment and the read out of the detector will be upgraded for a new T-violation experiment (E06) at J-PARC. Details of the gamma-ray detector and updated simulation results are described later.

2 Existing experimental results

There is no conclusive experimental results at this moment for ω meson. Some experiments have been performed to measure mass modification of other vector mesons.

The KEK-PS E325 experiment [10] measured the e^+e^- decays of light vector mesons ($\rho/\omega/\phi$) made by the 12-GeV proton induced reaction in target nucleus. Their results show 9% decreasing of ρ meson mass. It can be expected that ω meson has the same mass decreasing as ρ , since both mesons have the same quark contents. However, ω peak is sitting on ρ 's broad peak and the measurement has small sensitivities for ω meson mass modification.

Recently, CLAS at J-Lab reported mass broadening of ρ meson in γA reactions, though they did not observe mass decreasing [11]. They have small sensitivities for ω meson mass modification due to the same reason as the KEK experiment.

As a comparison between two experiments, it should be noted that the initial condition of generated ω meson is important, since the difference between CLAS and KEK results can be understood as the difference of production process. Thus, the initial condition of ω meson need to be determined simultaneously and the current proposed experiment will give such measurements.

Mass spectral of ω meson in nucleus were measured by the CBELSA / TAPS experiment in $\pi^0\gamma$ decay channel in γA reactions [6]. Since ρ mesons have a very small branching ratio (6.0×10^{-4}) to $\pi^0\gamma$ decays, contribution of ρ meson is negligible in this measurement. Originally, they claims 14% decreasing of ω mass [6]. However, obtained spectra are slightly changed [12] as shown in Fig.3 and there is no evidence for mass modification at this moment. Updated mass shape for Nb target is consistent with one for LH₂ target. Momentum range of ω mesons measured by TAPS is too high to detect mass modification.

To detect mass modification of ω meson in nuclei, we need to measure mass spectra of ω mesons decayed inside nuclei. The fraction of mesons decayed inside nucleus strongly depends on their momentum and decay width in nucleus. K. Gallmeister *et al.* calculated mass spectra of ω meson for TAPS experiment with and without mass modification using Gi-BUU transport model [13]. As a results, there is very small difference between those spectra, since very small fraction of generated ω meson decayed into $\pi^0\gamma$ inside nucleus.

What we have learn from TAPS results is that ω mesons with small momentum need to be detected and effects of decay width in nucleus need to be carefully taken into account for yield evaluation. For the first point, we focus on almost stopped ω mesons (less than 50 MeV/c). This condition is

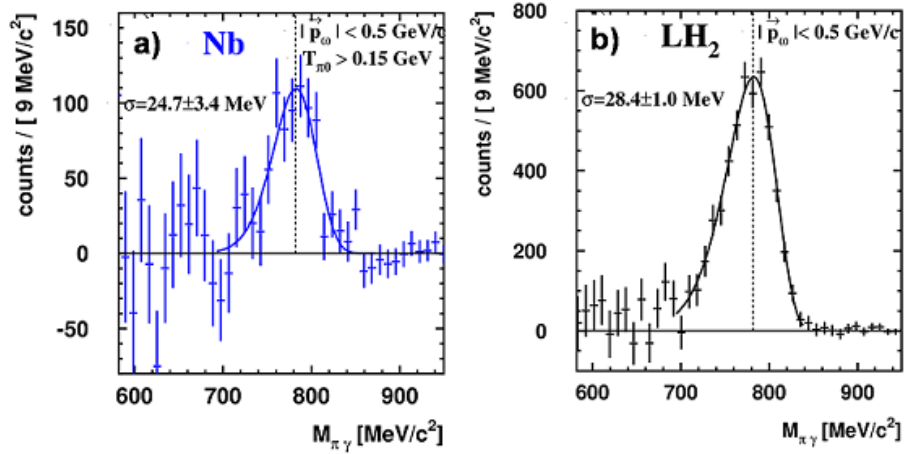


Figure 3: Updated mass spectra of ω meson after background subtraction for (a) Nb target and (b) LH₂ target [12].

achieved by combined measurements of forward neutron and ω meson decays.

Another issue is large width of ω meson in nucleus. The TAPS group reported larger decay width in nucleus due to interactions between ω mesons and nucleus [14]. As shown in Fig.4, based on measured transparency factor by TAPS experiment, total width of ω meson in the nuclear medium is evaluated. The calculation need to be extrapolated to lower momentum region, since our target momentum region is less than 50 MeV/ c and TAPS does not cover the lower momentum region. Normalized BUU calculation (red line) is used for the extrapolation. The BUU calculation takes into account known hadronic interactions and uses ω N interaction cross section measured by TAPS as input. As shown in Fig.4, the width of 60 MeV/ c^2 can be applied for the momentum region of less than 50 MeV/ c . Thus, the branching ratio of $\pi^0\gamma$ decays in nucleus becomes 1.5% of total decays instead of 8.92% in free space.

As shown in Fig.2, assumed potential in the calculation of H. Nagahiro *et al.* is consistent with the TAPS and BUU evaluation. H. Nagahiro *et al.* assumed 29 MeV/ c^2 for imaginary part of the potential and it corresponds to the width of 58 MeV/ c^2 . The calculation of H. Nagahiro *et al.* is for generation of ω meson and takes into account several nuclei effects. Thus, we estimate our final yield based on their calculation. Details of our estimation are described later.

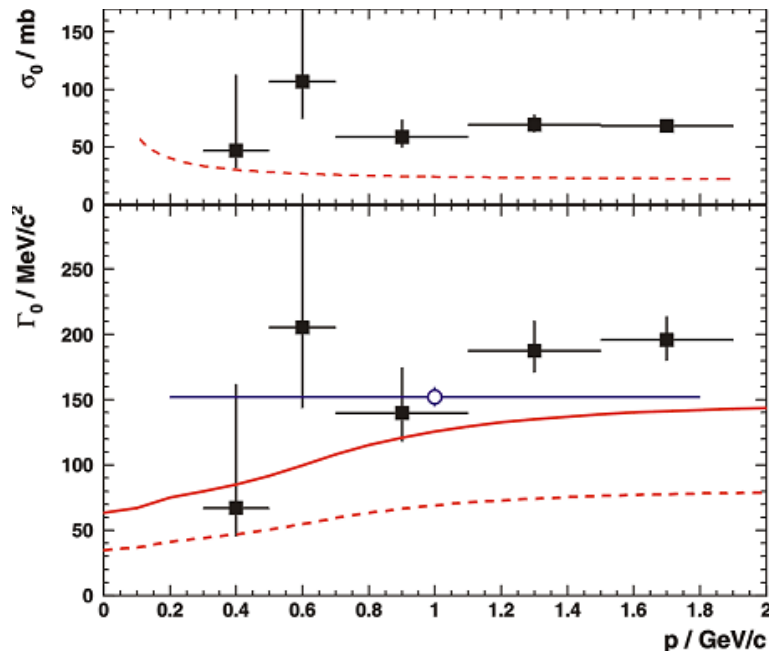


Figure 4: Figure and caption are taken from [14]. Upper part: The inelastic ωN cross section extracted from the Glauber analysis (data) in comparison to the inelastic cross section used in the BUU simulation [15]. Lower part: Width of the ω meson in the nuclear medium in the nuclear rest frame as a function of the ω momentum in a Glauber analysis (squares), from the Giessen BUU model with the inelastic cross section from the upper figure (red dashed line), and after fit to the TAPS data with BUU [solid gray (red) line], and the Valencia Monte Carlo simulation (blue circle), respectively.

3 Neutron counter

In the previous proposal, a neutron counter has $50\text{mm}\times 50\text{mm}\times 300\text{mm}$ scintillators and an acceptance for forward neutron is about $\pm 1^\circ$. Larger neutron counter is needed to have enough yield, since strong absorption of ω mesons in nucleus can be occurred. Now the neutron counter has $100\text{mm}\times 30\text{mm}\times 600\text{mm}$ scintillators and the acceptance is about $\pm 2^\circ$. A schematic view of neutron counter is shown in Fig.5. Momentum transfers as a function of the incident π^- momentum in the $p(\pi^-,n)\omega$ reaction are shown in Fig.6. Small momentum transfer can be kept with updated detector. To see a bound state, small momentum transfer is essential. Also, we will have a specified trigger to find a bound state (see section 8). With the trigger, large statistics can be collected.

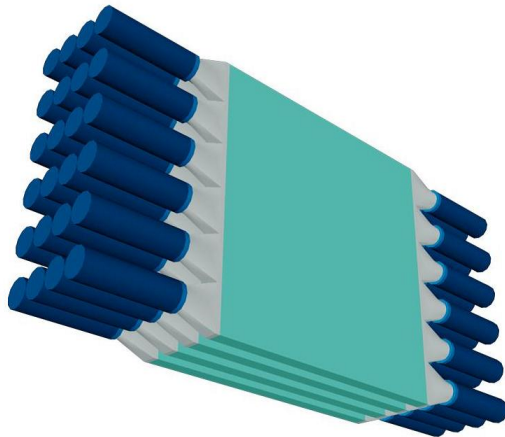


Figure 5: Schematic view of neutron counter.

3.1 Beam test for large scintillator

We performed a beam test at LNS GeV- γ beam line (Tohoku University) for a $100\text{mm}\times 30\text{mm}\times 600\text{mm}$ BC408 scintillator to see performance of the large scintillator matches our requirements, i.e. 80ps of time resolution. As a result, 56ps of time resolution is obtained, as shown in Fig.7.

A time lag between both ends of PMTs is shown in Fig.8. Three incident points on the scintillator were measured: center, 10cm shifted from the center and 20cm shifted from the center. A position resolution is decreasing as a particle incidents near the edges of scintillator. However, this effect does not affect to the time resolution after slewing corrections with charge information.

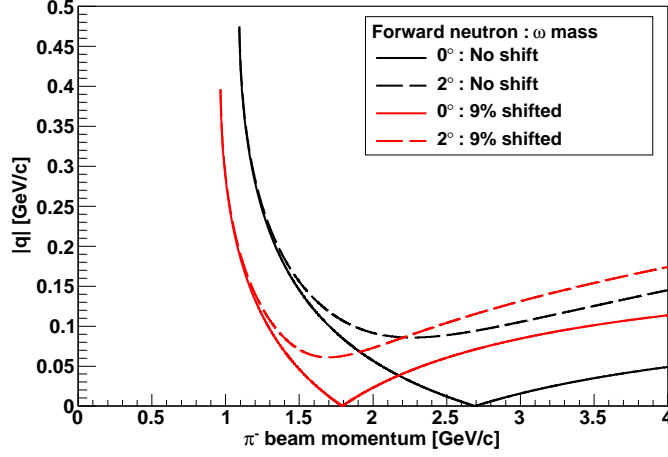


Figure 6: Momentum transfers as a function of the incident π^- momentum in the $p(\pi^-,n)\omega$. The solid and dashed lines show the momentum transfers with forward neutron detection angle 0° and 2° respectively. The red lines indicate when the ω mass shifts 9%.

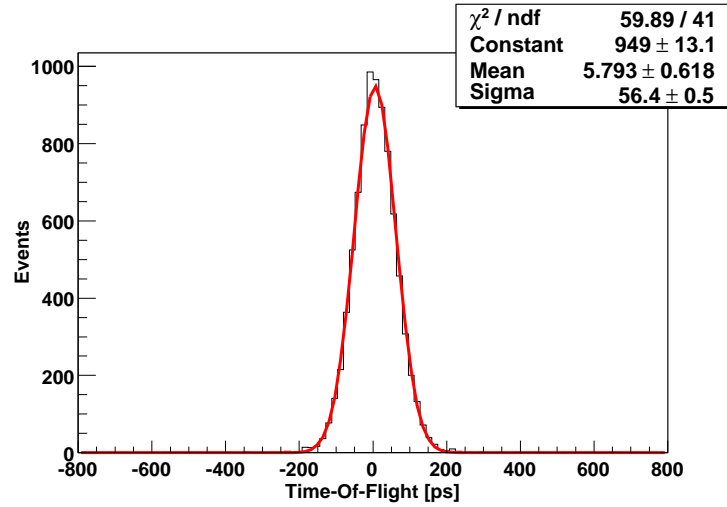


Figure 7: A spectrum of time-of-flight (TOF) at LNS beam test. 56ps time resolution is achieved as a result. It is enough for 80ps time resolution of required performance.

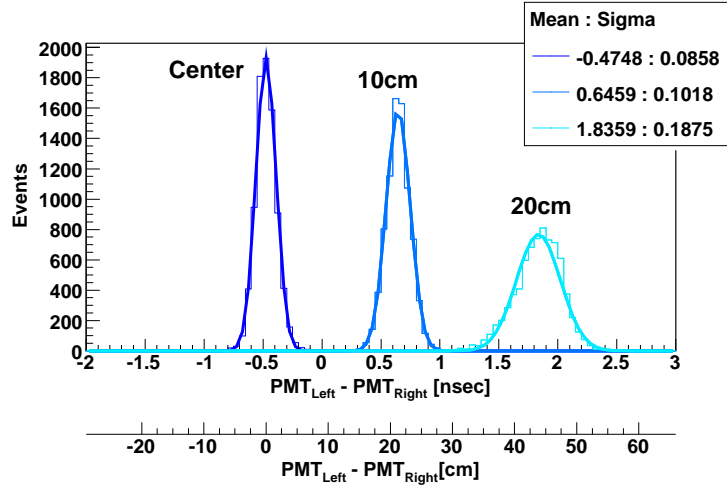


Figure 8: Histograms of position resolution for a $100\text{mm} \times 30\text{mm} \times 600\text{mm}$ scintillator. It indicates that the position resolution decreases as a particle incidents near the edges of scintillator. Difference of light propagation length between left and right PMT is shown under the horizontal axis. The light propagation length calculated with a light velocity and a refractive index of the scintillator.

3.2 Neutron detection efficiency

In the previous proposal, lead plates are used for neutron conversion materials. As a result of a Monte Carlo simulation used FLUKA package, iron plates have similar efficiency with lead plates. Then, we decide to use iron plates as a neutron converter, since iron plates have reasonable cost. Energy distributions of produced particles by neutron from the iron plates of 10mm thickness by neutron are shown in Fig.9.

Particle emission probabilities are summarized in Table 1. When all emitted protons are detected with the scintillators, 23.3% of neutron efficiency is achieved using 4 layers. Scintillator's own efficiency of 2.5% with 4 layers is also included.

A schematic view of cross section of the neutron counter with iron plates is shown in Fig.10.

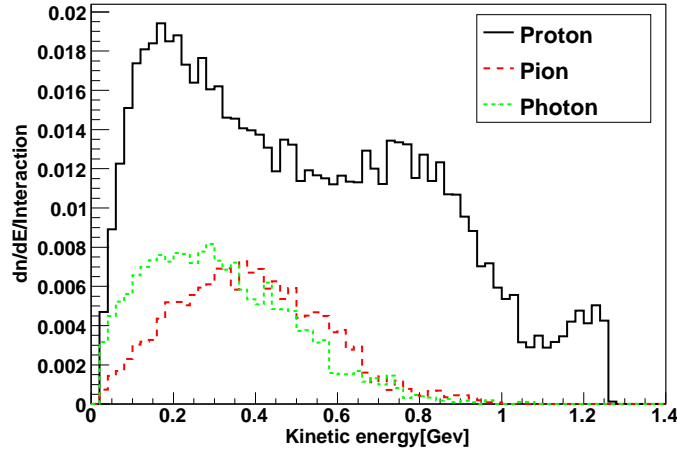


Figure 9: Energy distributions of produced particles from the iron plate 10mm thick by neutron.

Table 1: Particle emission probabilities

Protons per one neutron	5.2 %
Pions per one neutron	1.2 %
Photons per one neutron	2.1 %

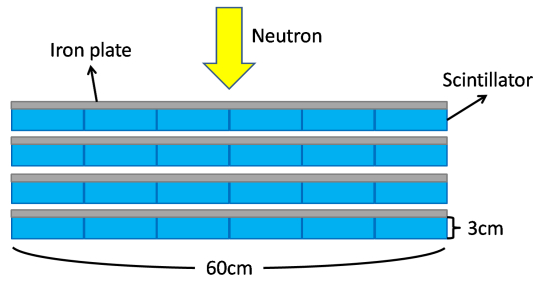


Figure 10: Schematic view of cross section of the neutron counter.

4 Gamma-ray detector and simulation study

We developed a fast simulation code to evaluate a realistic mass resolution of a gamma-ray detector. An energy resolution, an angular resolution and a shower leak at a crystal have been considered on the code. At first, the code is tuned to reproduce existing experiment data. Then, we simulate for ω meson mass reconstruction using this code.

4.1 Existing data

Existing experiment data are obtained from stopped kaon decay [16, 17]. These data are shown in Fig.11 to Fig.13, and obtained resolutions are in the caption of figures and summarized in Table 2.

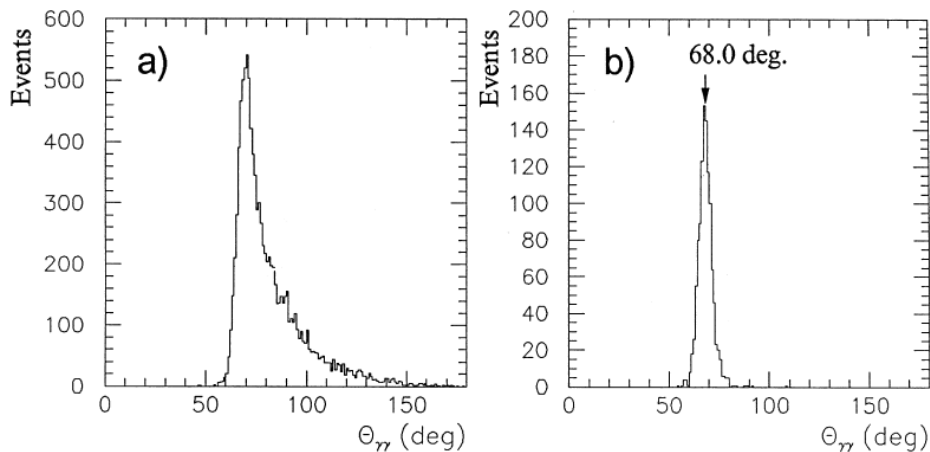


Figure 11: Measured distribution of an opening angle between two photons from π^0 in $K^+ \rightarrow \pi^+\pi^0$ decays: (a) all $K^+ \rightarrow \pi^+\pi^0$ events are shown; (b) events with $(E_1 - E_2)/(E_1 + E_2) \leq 0.1$ are presented. The minimum opening angle of 68.03 is obtained.

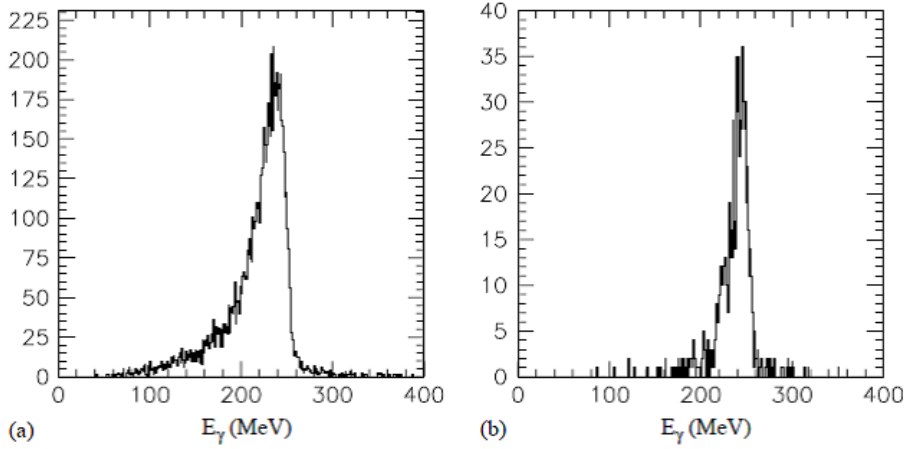


Figure 12: Energy sum of two photons from the π^0 in $K^+ \rightarrow \pi^+\pi^0$ decays. (a) All events with peak value $E_{\gamma\gamma} = 235.7$ MeV, $\sigma = 5.2\%$. The low energy tail is due to the shower leakage into muon and beam holes. (b) Photons are detected away from muon holes. $E_{\gamma\gamma} = 242.5$ MeV, $\sigma = 4.1\%$.

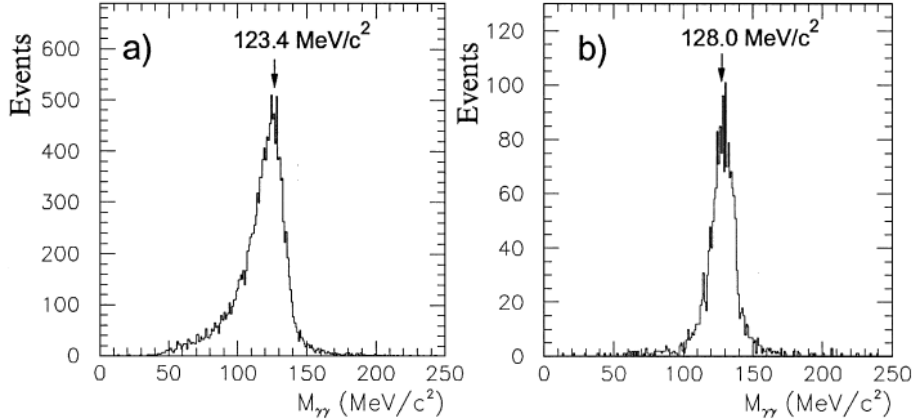


Figure 13: Invariant mass of $\gamma - \gamma$ events from $K^+ \rightarrow \pi^+\pi^0$ decays; (a) all events reconstructed in the π^0 detector; (b) events detected away from the muon holes area.

4.2 Simulation tuning

In the reference data, a stopped K^+ decays into π^0 and π^+ , and the π^0 also decays into 2 γ 's. On our simulation, the reaction is simulated and γ 's are

detected by the gamma-ray detector. The geometry of gamma-ray detector is shown in Fig.14. The detector is used for KEK E246 experiment. An energy resolution, an angular resolution and shower leaks at crystals are tuned to fit the existing data. As a base characteristics of the detector, the gamma-ray detector has the 4.3% energy resolution σ_E/E at 100 MeV and 2.8% at 200 MeV [16]. We assume that the energy resolution can be understood as a quadratic sum of energy dependent part and constant part, and the function of the energy resolution is shown in Fig.15. The mark, \oplus , represents addition in quadrature: $\frac{\sigma_E}{E} = \frac{a}{\sqrt{E}} \oplus \frac{b}{E}$ represents $\left(\frac{\sigma_E}{E}\right)^2 = \left(\frac{a}{\sqrt{E}}\right)^2 + \left(\frac{b}{E}\right)^2$

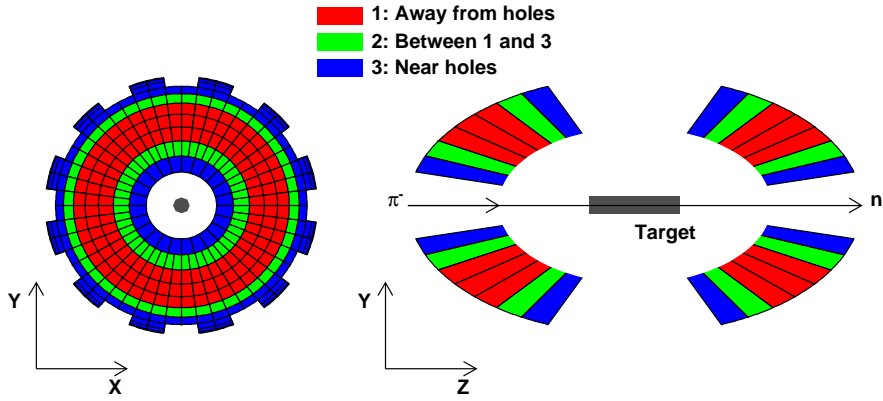


Figure 14: Schematic view of gamma-ray detector. Red parts and blue parts are the crystals which away from holes and near the holes respectively. Green parts are the crystals between red and blue parts.

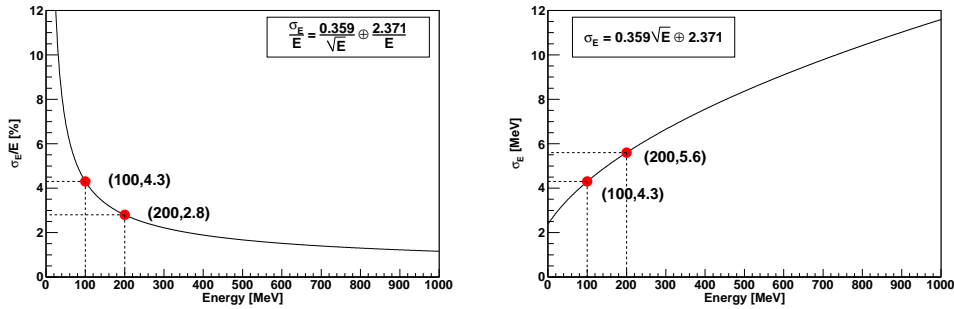


Figure 15: Assumed energy resolution function of gamma-ray detector. \oplus represents addition in quadrature.

To evaluate shower leak effects of the detector, the leak effects of γ 's are

parameterized as shown in Fig.16 and Fig.17. Fig.16 shows the effects of longitudinal leaks. Light absorption values are described as an electromagnetic cascade, like,

$$\begin{aligned} \text{Light absorption} &= \frac{1}{E_0} \int_0^t \frac{dE}{dt} dt \\ &= \frac{1}{E_0} \int_0^t b \frac{(bt)^{a-1} e^{-bt}}{\Gamma(a)} dt, \end{aligned} \quad (1)$$

here,

$$\begin{aligned} t &= x/X_0 = \text{depth in radiation lengths}, \\ b &\approx 0.5, \\ a &= b(\ln y + 0.5) + 1, \\ y &= E_\gamma/E_c. \end{aligned}$$

x is length of crystal, X_0 is radiation length: 1.85 cm for CsI(Tl) crystals, E_c is critical energy for electrons: 11.17 MeV and E_γ is induced photon energy.

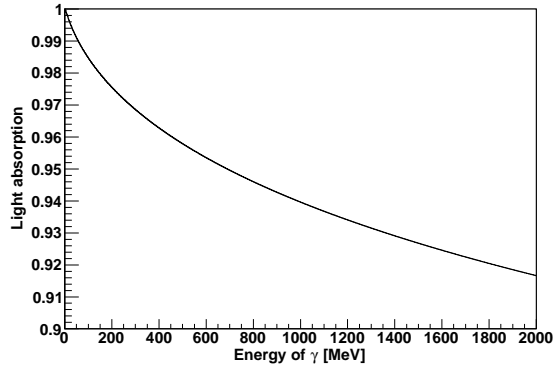


Figure 16: Longitudinal leaks as function of E_γ [MeV].

In addition to the longitudinal leaks, there are additional energy smearing and horizontal leaks as shown in Fig.17. A gaussian is used for the γ 's which has only longitudinal leaks and additional smearing, and a landau distribution for the γ 's which hit near holes and have horizontal leaks. Additional smearing effect is caused by calibration issues and tuned to fit existing data.

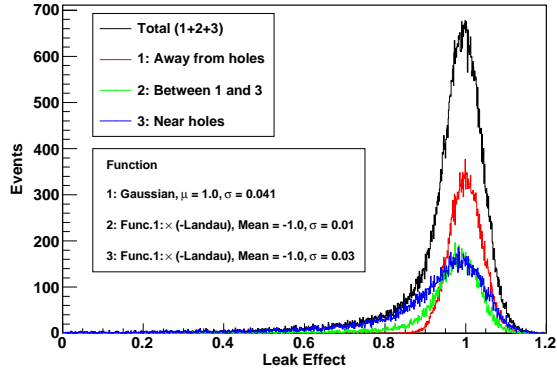


Figure 17: Effect of shower leak at crystals. Red, blue and green color are linked the colors in Fig.14.

Simulation histograms are shown in Fig.18 to Fig.20, and obtained results are summarized in Table 2.

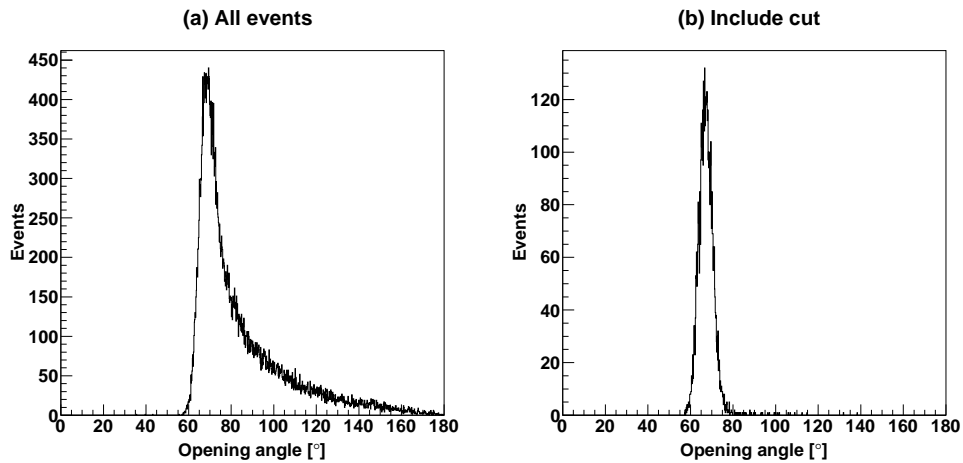


Figure 18: Simulated distribution of an opening angle between two photons from π^0 in $K^+ \rightarrow \pi^+\pi^0$ decays. All $K^+ \rightarrow \pi^+\pi^0$ events are shown in (a). Events with $-0.1 \leq (E_1 - E_2)/(E_1 + E_2) \leq 0.1$ are presented in a (b). The minimum opening angle of 67.1 is obtained.

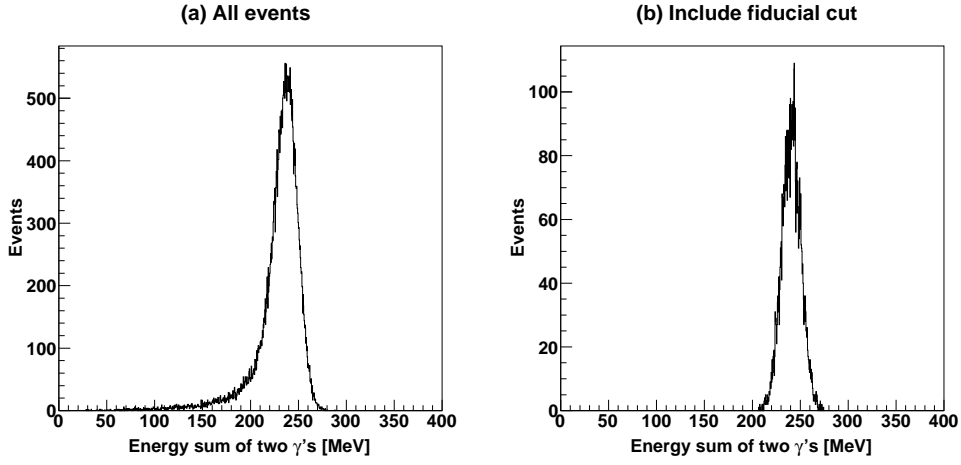


Figure 19: Simulated energy sum of two photons from the π^0 in $K^+ \rightarrow \pi^+\pi^0$ decays. All events with peak value $E_{\gamma\gamma} = 236.1\text{MeV}$, $\sigma = 5.2\%$ are shown in (a). The low energy tail is reproduced as Fig.12. (b) Photons are detected away from muon holes (fiducial cut, see section 4.3). $E_{\gamma\gamma} = 240.5\text{MeV}$, $\sigma = 4.0\%$.

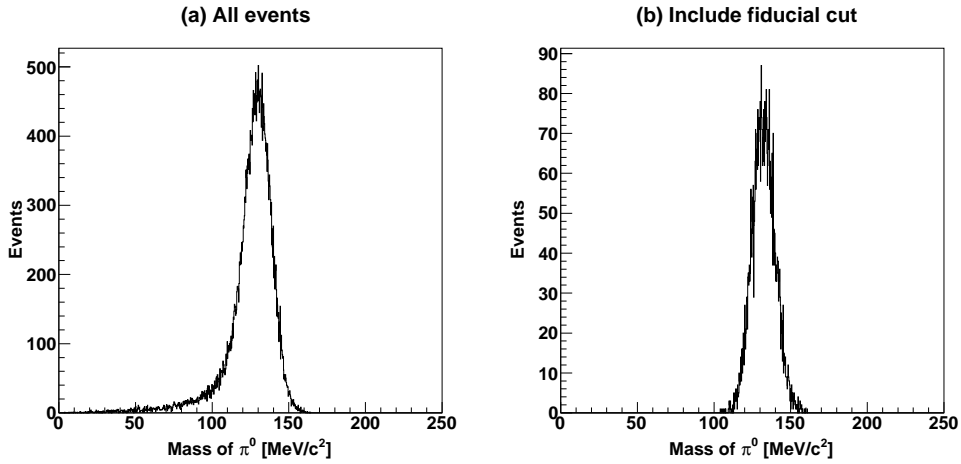


Figure 20: Simulated invariant mass of π^0 from $K^+ \rightarrow \pi^+\pi^0$ decays. All events with $m_{\pi^0} = 129.2\text{MeV}/c^2$ and $\sigma = 7.0\%$ are shown in (a). Events detected away from the muon holes area are shown in (b). $m_{\pi^0} = 132.5\text{MeV}/c^2$, $\sigma = 5.6\%$

Table 2: Summary of existing data and simulation

	Existing data	Simulation
The minimum opening angle [°]	68.03 [16]	67.1
Energy sum of two photons		
Peak value of all events [MeV]	235.7 [17]	236.1
σ [%]	5.2 [17]	5.2
Peak value of away from holes [MeV]	242.5 [17]	240.5
σ [%]	4.1 [17]	4.0
Invariant mass of π^0		
Peak value of all events [MeV/c ²]	123.4 [16]	129.1
σ [%]	6.7 [17]	7.0
Peak value of away from holes [MeV/c ²]	128.0 [16]	132.5
σ [%]	5.6 [17]	5.6

As shown in Table 2, our simulation is in excellent agreement with existing data.

4.3 Fiducial cut

As shown in Fig.19 and Fig.20, a large tail is observed for γ 's hit near holes. This tail can be a serious background of our measurements such as $\omega \rightarrow \pi^0\gamma$ decays. Thus, additional fiducial cut must be applied. To detect direct γ 's from ω decays, we use only red crystal in Fig.14. For γ 's from π^0 decays, all crystals are used for detection. Without fiducial cuts, it's hard to distinguish mass modification of ω and experimental effects. To check this fiducial cut effects, we will collect high momentum ω decays, which don't have mass modification effects.

4.4 Invariant mass evaluation

Invariant mass spectra of ω meson are simulated. Results are shown in Fig.21. A good mass resolution can be achieved. However, a large tail in the left side of omega peak without the fiducial cut. This region is exactly the same region which we can expect our physics signals and we need to eliminate this tail. We choose events that γ 's from $\omega \rightarrow \pi^0\gamma$ decays hit away from muon holes (fiducial cut, see section 4.3). After applying the fiducial cut, the ω mass tail is absent as shown in Fig.21(b).

Fig.22 shows invariant mass spectra when the muon holes of the gamma-ray detector are covered with CsI(Tl) crystals.

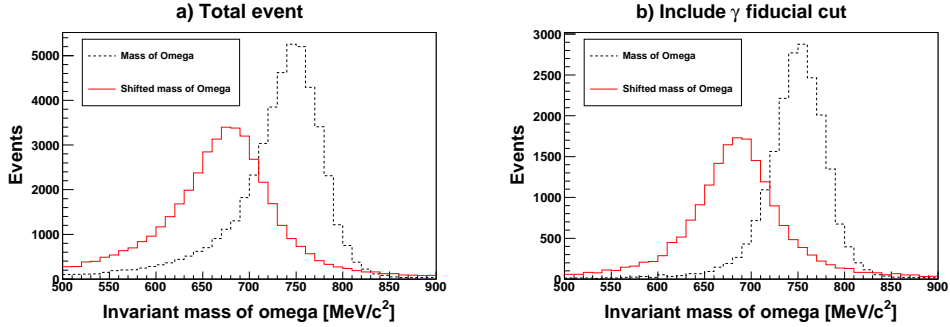


Figure 21: Invariant mass of ω meson smeared by energy resolution, angular resolution and shower leak of gamma-ray detector. Two lines represent ω mass shift = 0 (dotted line), 9% (red solid line). Mass decreasing of 9% is measured at KEK-E325. (a) All events. (b) A Fiducial cut for γ produced $\omega \rightarrow \pi^0\gamma$ reaction is included.

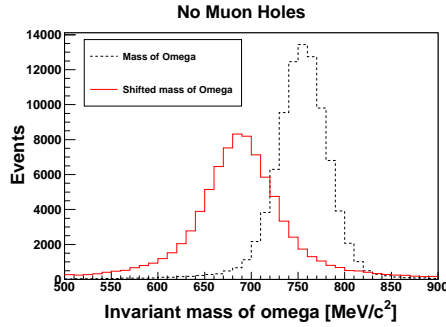


Figure 22: Invariant mass of ω meson with gamma-ray detector which has no muon holes. Two lines represent ω mass shift = 0 (dotted line), 9% (red solid line).

When the muon holes are covered with CsI(Tl) crystals, mass tails are eliminated clearly.

4.5 Detector acceptance

The gamma-ray detector has a barrel structure that covers about 77.5% of 4π . According to our simulation, the acceptance of ω decays is 44.9%. After applying the fiducial cuts, 19.9% of ω mesons are survived.

In addition, 0.6% of 2 γ 's showers are merged and not distinguishable. It should be taken into account as an additional loss.

When the muon holes are covered with crystals, the gamma-rays detector has the geometry covered about 96.6% of 4π . We have 89.3% of the ω event acceptance and 82.7% after applying the fiducial cut.

Table 3: Summary of the detector acceptance

	With muon holes	No muon holes
Geometry	77.5%	96.6%
ω event	44.9%	89.3%
Fiducial cut	19.9%	82.7%
2γ merging	0.6%	1.2%

5 Yield and mass spectrum

We evaluate expected yield from a theoretical calculation based on measured cross sections. Then, expected missing mass spectra and expected invariant mass spectra are calculated.

5.1 Theoretical cross section calculation

Obtained ω yield is estimated with measured cross section in $p(\pi^-,n)\omega$ reaction [18]. Fig.23 shows a summary plot of cross sections of backward ω production as function of $\cos\theta_\omega$ [19]. H. Nagahiro *et al.* calculated the energy spectra based on the above experimental cross section and known nuclear effects as shown in Fig.2. The calculated spectrum is decomposed to two parts, such as conversion part and escape part, as shown in Fig.24. The calculation is done with a ^{12}C target and an attractive potential $V_\omega(r) = -(156+29i)\frac{\rho(r)}{\rho_0}$. The potential V_ω is consistent with TAPS result [14]. The ω meson interacted with nuclei is presented as a conversion (green line). The ω meson which does not interacted with nuclei and escaped from nuclei is presented as an ω escape part (blue line). As described before, green line has a large width and only small fraction (1.5%) of ω decays into $\pi^0\gamma$. The total events are shown in a red line. An incident pion momentum of 1.8GeV/c is used in the calculation.

Based on the calculation, the expected yield and mass spectra are evaluated including several experimental effects.

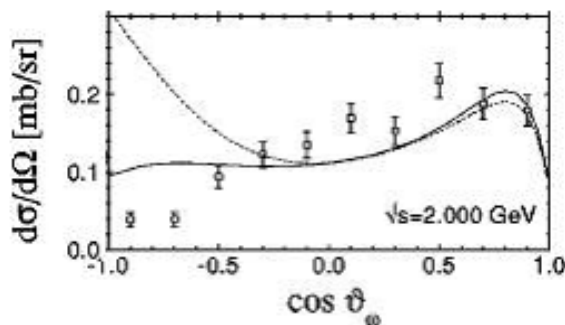


Figure 23: Summary plot of differential cross section of ω production as function of $\cos\theta_\omega$ [19]. Points represent measurements. Lines represent theoretical calculations.

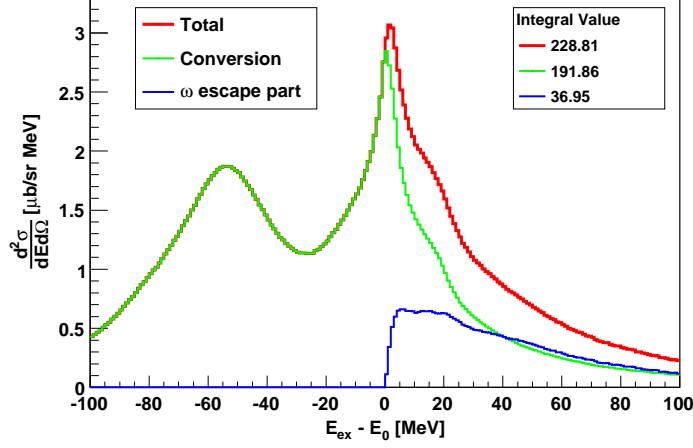


Figure 24: Calculated spectra of $^{12}\text{C}(\pi^+,p)^{11}\text{C}\otimes\omega$ reaction cross section as functions of the excited energy E_{ex} [9]. An incident pion momentum is $1.8\text{GeV}/c$. E_0 is the stopped ω energy; 782MeV .

5.2 Yield calculation

For yield calculation, we use an eq.(2) and parameters summarized in Table 4. An expected yield is shown in Fig.25. The spectrum does not contain smearing effect from experimental resolutions. The conversion and the ω escape part are presented as green line, and blue line, respectively. The total events are also shown in the red line. It indicates that 4300 total events and 1800 shifted mass events are expected per 100 shifts.

$$Y = \frac{d^2\sigma}{dE d\Omega} \times BtoS \times I \times t \frac{\rho}{A} N_A \times AFN \times EFN \times RLT \times FSI \times SPS \times BR \times E3G \quad (2)$$

Y : Yield [/MeV 100shifts]

$\frac{d^2\sigma}{dE d\Omega}$: [$\mu\text{b}/\text{sr MeV}$] as shown in Fig.24

Table 4: Parameters of yield calculation eq.(2)

Parameter	Value	
$BtoS$	10^{-30}	$\mu\text{b} \rightarrow \text{cm}^2$
I	10^7	Beam intensity [/Spill]
t	6	Target thickness [cm]
ρ	2.267	Target density (Carbon) [g/cm^3]
A	12.01	Atomic weight (Carbon) [g/mol]
N_A	6.022×10^{23}	Avogadro constant [/mol]
AFN	3.828×10^{-3}	Acceptance of Forward Neutron [sr]
EFN	25	Efficiency of Forward Neutron [%]
RLT	0.89	Radiation loss in target (11%)
FSI	0.6	Without final state interaction
SPS	480000	Spills per 100 shifts
BR	-	Branching ratio $\omega \rightarrow \pi^0\gamma$
	0.089	for at free space (blue line in Fig.24)
	0.015	for inside nuclear (green line in Fig.24)
$E3G$	0.45	Efficiency of 3 γ 's events

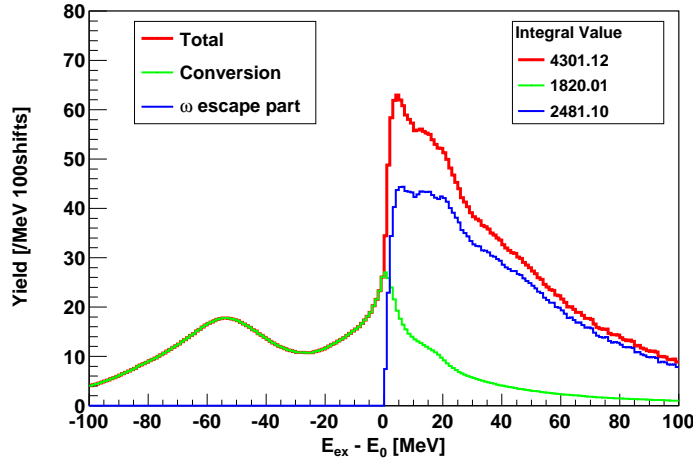


Figure 25: Estimated yield calculated from Fig.24 and eq.(2). It indicates that 4300 total events and 1800 shifted mass events are expected per 100 shifts.

5.3 Expected missing mass spectrum

An expected energy spectrum of ω which smeared by 80ps of time resolution of the neutron counter is shown in Fig.26. Also, the expected missing mass spectrum is shown in Fig.27. We assume that the neutron counter has 80ps time resolution and the neutron flight path is 7m in this evaluation. On the energy spectra, bound resion can be selected as $E_\omega < E_0$.

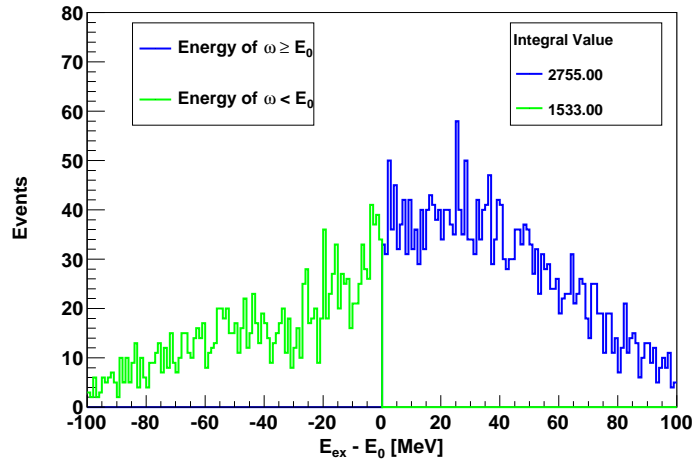


Figure 26: Expected energy spectrum of ω . It is calculated from Fig.25 and includes the 80ps time resolution of the neutron counter. E_0 is the stopped ω energy.

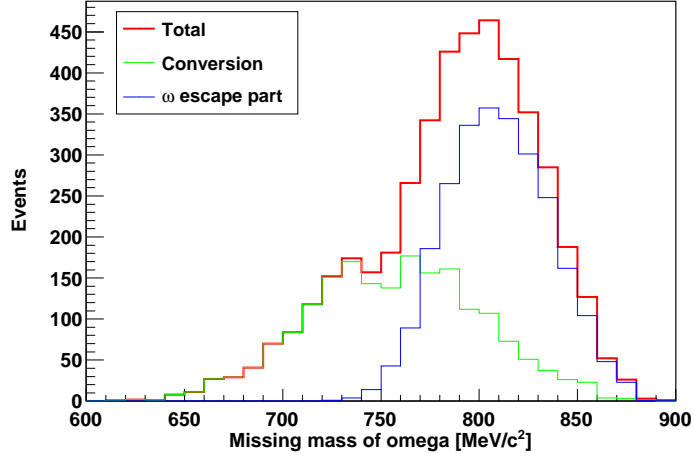


Figure 27: Expected missing mass spectrum.

If we don't require 3 γ 's decay coincidence, so we use only neutron counter, more events can be expected as shown in Fig.28 and Fig.29

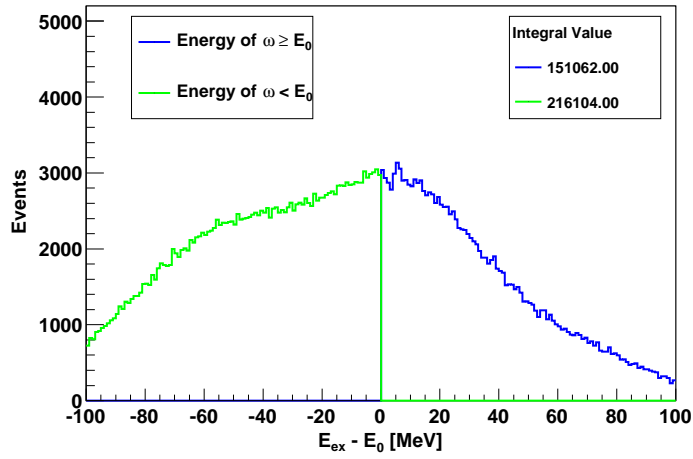


Figure 28: Expected energy spectrum of ω without 3 γ 's decay coincidence. It includes the 80ps time resolution of the neutron counter. E_0 is the stopped ω energy.

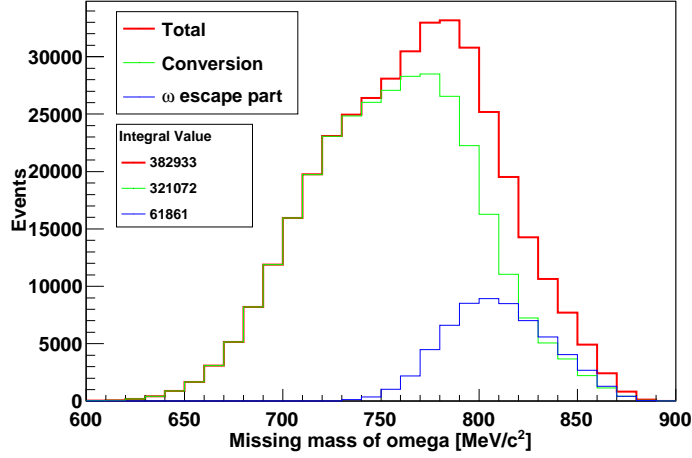


Figure 29: Expected missing mass spectrum without 3 γ 's decay coincidence.

5.4 Expected invariant mass spectrum

An expected invariant mass spectrum is calculated and shown in Fig.30. We assume that the conversion part (green line in Fig.27) has 9% decreased ω mass and the omega escape part (blue line in Fig.27) has no shifted ω mass. Using energy of ω measured by forward neutron, the spectrum can be decomposed two parts, such as bound region (green) and no-bound region (blue). The total events are shown in Fig.30 (a) red line.

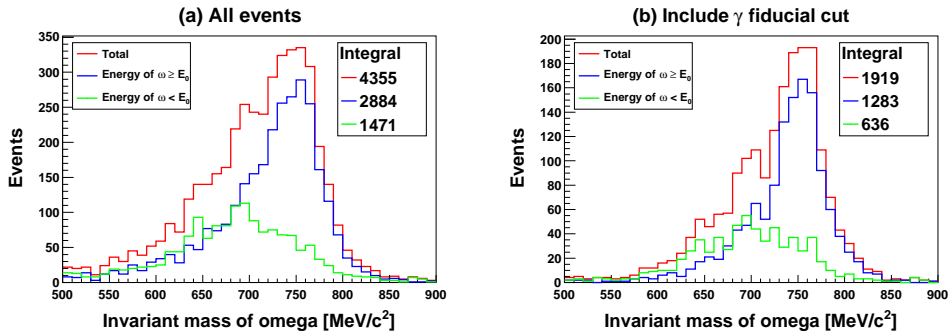


Figure 30: Expected invariant mass spectrum.

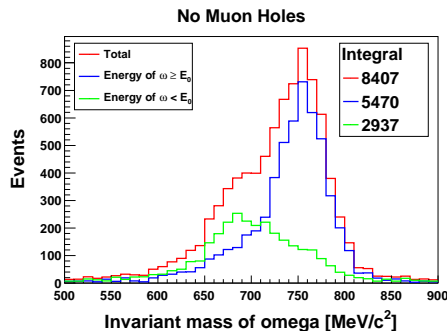


Figure 31: Expected invariant mass spectrum when the gamma-ray detector has no muon holes.

Applying a cut of $E_\omega < E_0$, the mass shifted part can be selected as shown in Fig.30 (a) (green line).

There is the ω mass tail due to shower leakage as shown in Fig.30 (a). We apply the fiducial cut, which is described in section 4.3, and eliminate the tail as shown in Fig.30 (b).

In fact, when we can fill all muon holes with additional crystals, clear spectrum can be obtained as shown in Fig.31. Still, blue line contains some tails, since there is a conversion part in the range of $E_\omega \geq E_0$.

5.5 Final yield for physics

Although 1800 events per 100 shifts are expected for mass shifted ω meson, 1500 events are survived with applying the cut of $E_\omega < E_0$. If the fiducial cuts are applied, 600 events per 100 shifts are expected for the shifted mass event.

When the muon holes are covered, 2900 events per 100 shifts are expected for the shifted mass event.

6 Background estimation

The main background in final plot comes from $p(\pi^-, n)2\pi^0$ reactions. The background in 3 γ 's measurements is 2 π^0 decays and 1 γ missing in the detection. Its probability is about 25%. In addition, we require that forward neutron has the momentum of 1.77 to 1.99, which corresponds to neutron momentum range of modified ω meson production. Combinatorial background is caused by non-correlated pairs and it can be subtracted using a mixed event method.

An expected final plot of invariant mass is shown in Fig.32. When we apply $E_\omega < E_0$ cut to see mass modification effects, the spectrum is shown in Fig.33. To separate the signal from the background, the 1 γ missing background have to be understood well. This can be estimated with 4 γ events and 14000 events of 4 γ events per 100 shifts can be collected with the current setup.

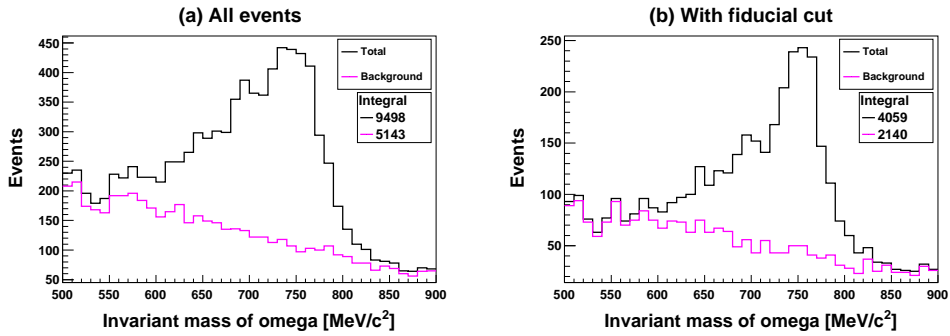


Figure 32: Final plot of invariant mass. Black and magenta lines represent total and background, respectively. (a) for all events. (b) for events applied fiducial cut.

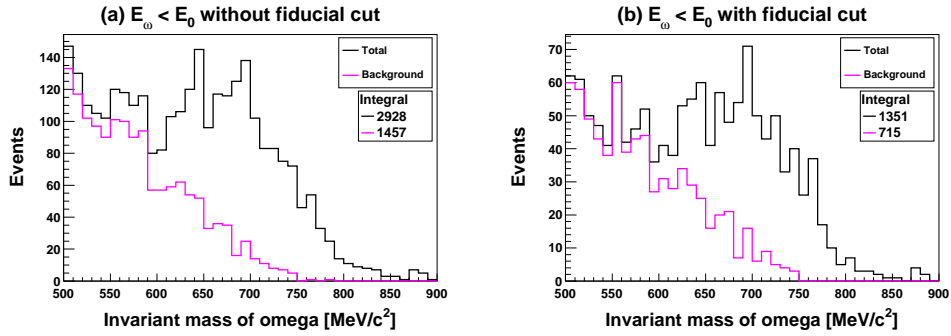


Figure 33: Final plot of invariant mass with $E_\omega < E_0$. Black and magenta lines represent total and background, respectively. (a) for all events. (b) for events applied fiducial cut.

When the muon holes of the gamma-ray detector are covered, background caused by 1 γ missing event are strongly suppressed as shown in Fig.34

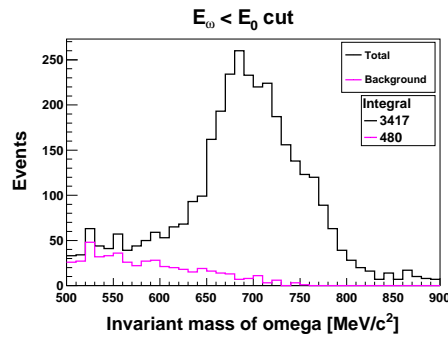


Figure 34: Final plot of invariant mass when the gamma-ray detector has no muon holes. The total events with $E_\omega < E_0$ cut are shown in black lines, and the backgrounds are shown in magenta lines.

7 Final state interaction

Another issue is the final state interaction of π^0 . It is evaluated for TAPS experiment using a transport model [20]. Fig.35 shows the calculation in [20]. According to this calculation, when π^0 meson is scattered in nucleus,

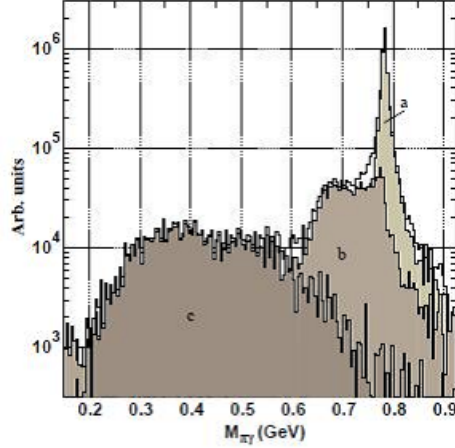


Figure 35: The $\pi^0\gamma$ mass distribution obtained from a Monte Carlo simulation of the process $\gamma + \text{Nb} \rightarrow \pi^0\gamma + X$ at $E_\gamma = 1.2$ GeV. The spectrum is decomposed into different contributions corresponding to the fraction of ω mesons decaying outside the nucleus (a), the fraction of ω mesons decaying inside for which the π^0 does not rescatter (b), and the fraction of ω mesons decaying inside the nucleus for which π^0 rescatters (c).

mass distribution of ω have very large shift in lower side, because π^0 meson scattering in nuclei is governed by δ dynamics and most of rescattered π mesons have small kinetic energy (< 150 NeV). This situation doesn't change between γA and πA reactions [21]. Thus, the effect in interested mass region, i.e. just below ω mass, is negligible. However, 40% of ω mesons have the final state π^0 rescattering in nucleus and final yield is decreased. To confirm the number, we are preparing the detailed calculations for πA reactions.

8 Trigger

Our main trigger is a coincidence of more than 2 γ 's in the calorimeter and one neutron detected at the forward counter. Although the ω decays contain 3 γ 's, it is difficult to separate 2 γ 's from π^0 decays at the trigger level. Then, main background at the trigger is $p(\pi^-, n)\pi^0$ reaction. Fig.36 shows measured total cross section for the reactions $\pi^-p \rightarrow X$.

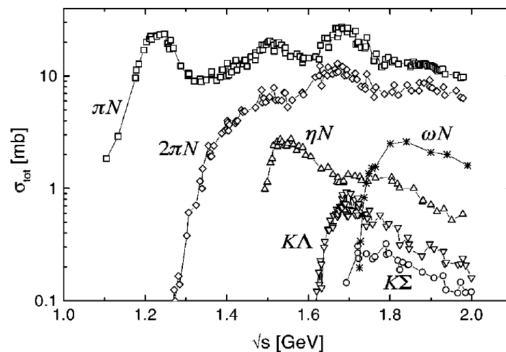


Figure 36: Total cross sections for the reactions $\pi^-p \rightarrow X$ with X as given in the figure [19].

The cross section of the π^0 production at the backward direction is also measured as 0.1 mb/sr (CM frame) [22]. In addition, $p(\pi^-, n)2\pi^0$ also exists and the cross section of the reaction is estimated as 0.06 mb/sr (CM frame). The angular distribution is measured at slightly lower beam momentum [23]. Finally, the main trigger rate becomes 20 events per spill.

In addition to the main trigger, we have several triggers for additional physics and calibrations. The second trigger requires only forward neutron hit to search ω bound states. To measure ω bound states, information of ω decays is not necessary, however, forward neutron measurements will have a huge background without ω decays information. For example, an experiment performed at BNL to search η bound state shows a continuum background of 0.1 mb /sr/MeV [24]. Then, the trigger rate will become 10 \sim 100 times larger than the main trigger and need to be prescaled to match DAQ band width.

Also, we have γ detection only trigger for calibration purpose. With the trigger, high momentum ω mesons can be detected and such ω mesons don't have a nuclear medium effect, since almost ω mesons are decayed outside nucleus. Experimental effects, such as shower leakage tails, can be checked with this trigger data.

9 Additional Target

In the current proposal, we use carbon target mainly, since the carbon target is suitable both for the bound state search and invariant mass measurements in nucleus. For future purpose, we are investigating for putting additional targets.

A liquid hydrogen target as a proton target is important to check our experimental effects and clearly demonstrate the modifications of ω mass in nuclei. We would like to have a liquid hydrogen target, however, space in the target region is limited and both the carbon and the liquid hydrogen target can't be placed at the same time. Thus, we give up the hydrogen target. To show mass modification and check our experimental effects, high momentum ω mesons are used. Still, we are planning to have a liquid hydrogen target in future.

Heavy nucleus targets, such as Ca and Nb, are suitable for measurements of ω meson mass modification, since a possibility of ω decaying inside nucleus becomes larger using larger nuclei. In addition, we can extract ω absorption cross section in nucleus from production cross sections of ω mesons and its target dependence. However, the bound state search becomes difficult, since there are many nucleon states and it's hard to identify ω bound state. We will put thin targets to measure absorption cross section.

10 Cost estimation

A brief cost estimation is shown in Table 5.

Table 5: cost estimation

Detector	element	description	Budget	cost [M Yen]
Beam Line	Tracker	MWPC	Common use	0
	Start Counter	Segmented scintillator	Common use	0
Neutron Counter	Frame		Grant(Kakenhi)	1
	PMT	48 x H2431	Grant(Kakenhi)	10
	Scintillator	24 pieces	Grant(Kakenhi)	2
CsI Calorimeter		Reuse of E06		0
	Additional Crystals Muon Hole	Fill Optional	Currently no supports	100
Total			13	
Total (Fill muon hole)			113	

To achieve the perfect experiment, we need to fill muon holes. However, without filling muon holes, we can have reasonable statics for modified ω meson.

11 Summary

We propose combined measurements of nuclear ω bound state and direct ω mass modification. Nuclear ω bound states are measured in $A(\pi^-, n)\omega$ reaction and decays of generated ω meson are also measured with $\omega \rightarrow \pi^0\gamma$ mode. Such exclusive measurement can supply essential information to establish mass modification of vector mesons in nucleus.

References

- [1] T. Hatsuda and S.H. Lee, Phys. Rev. **C46** (1992) R34.
- [2] T. Hatsuda and T. Kunihiro, Phys. Rep. **247** (1994) 221.
G.E. Brown and M. Rho, Phys. Rep. **269** (1996) 333.
W. Cassing and E.L. Bratkovskaya, Phys. Rep. **308** (1999) 65.
- [3] F. Klingl, N. Kaiser and W. Weise, Nucl. Phys. **A624** (1997) 527.
F. Klingl, N. Waas and W. Weise, Nucl. Phys. **A650** (1999) 299.
- [4] M.F.M. Lutz, Gy. Wolf and B. Friman, Nucl. Phys. **A706** (2002) 431.
- [5] P. Muehlich *et al.* , Nucl. Phys. **A780** (2006) 187.
- [6] D. Trnka *et al.* , Phys. Rev. Lett. **94** (2005) 192303.
- [7] M. Kaskulov *et al.* , Phys. Rev. **C75** (2007) 064616.
- [8] E. Marco and W. Weise, Phys. Lett **B502** (2001) 59.
- [9] H. Nagahiro, D. Jido, and S. Hirenzaki, Nucl. Phys. **A761** (2005) 92.
H. Nagahiro, D. Jido, S. Hirenzaki, e-Print: arXiv:0811.4516 [nucl-th].
H. Nagahiro, private communication.
- [10] K. Ozawa *et al.* , Phys. Rev. Lett **86** (2001) 5019.
M. Naruki *et al.* , Phys. Rev. Lett **96** (2006) 092301.
R. Muto *et al.* , Phys. Rev. Lett **98** (2007) 042501.
- [11] C. Djalali *et al.* , J. Phys. **G34** (2007) S495.
- [12] V. Metag *et al.* , JPS-DNP at Hawaii presentation
- [13] K. Gallmeister *et al.* , Prog. Part. Nucl. Phys. **61** (2008) 283.
- [14] M. Kotulla *et al.* , Phys. Rev. Lett **100** (2008) 192302.
- [15] P. Muhlich *et al.* , Eur. Phys. J. A **20** (2004) 499.
- [16] D.V. Dementyev *et al.* , Nucl. Instrum. Meth. **A440** (2000) 151.
- [17] Yu.G. Kudenko, Nucl. Instrum. Meth. **A494** (2002) 318.
- [18] J. Keyne *et al.* , Phys. Rev. **D14** (1976) 28.
- [19] G. Penner and U. Mosel, Phys. Rev. **C65** (2002) 055202.

- [20] J.G. Messchendorp, A. Sibirtsev, W. Cassing, V. Metag, and S. Schandmand, Eur. Phys. J. **A11**, 95-103 (2001))
- [21] V. Metag, private communication
- [22] J. E. Nelson *et al.* , Phys. Lett **B47** (1973) 281.
- [23] S. Prakhov *et al.* , Phys. Rev. **C69** (2004) 045202.
- [24] R.E. Chrien *et al.* , Phys. Rev. Lett. **60** (1988) 2595.